ChemistrySelect

Research Article
doi.org/10.1002/slct.202503583

Chemistry Europe
European Chemical Societies Publishing

www.chemistryselect.org

Synthesis, Characterization, and Anticancer Activity of Rhodium (III) Complexes with Bidentate and Tridentate N-Donor Ligands

Haoran Liang,*[a] Huan Hong,[a] Gang Wang,[b] Li Gao,[a] Shui Wang,[a] Yan Shen,*[a] and Yuanqiang Wang*[a]

A series of five novel rhodium(III) complexes of the type $[Rh(tpy)(N^{\wedge}N)Cl](PF_6)_2$, incorporating a tridentate 2,2′:6′,2″-terpyridine (tpy) ligand and various bidentate N-donor ligands, were synthesized and fully characterized. The single-crystal X-ray diffraction analysis of complex **5** $[Rh(tpy)(dppz)Cl](PF_6)_2$ (dppz = dipyrido[3,2-a:2′,3′-*c*]phenazine) confirmed its octahedral geometry. Cytotoxicity assays revealed potent antiproliferative activity against four human cancer cell lines (AGS, MCF-7, HeLa, and HepG2). Notably, complex **5** demonstrated enhanced selectivity and cytotoxicity toward AGS cells compared to cisplatin. Molecular docking studies indicated that complexes **3** and **5** effectively insert into the minor groove of calf thymus DNA (ctDNA), supported by favorable steric and electrostatic interactions. Mechanistic studies further confirmed that complex **5** induces apoptosis, causes S-phase cell cycle arrest, and elevates intracellular ROS levels in AGS cells. Collectively, these results highlight the potential of terpyridine-based Rh(III) complexes as promising scaffolds for metal-based anticancer drug development.

1. Introduction

Cancer remains a major global health challenge, imposing a significant burden on individuals and healthcare systems worldwide.[1] Chemotherapy continues to be a cornerstone of cancer treatment, with platinum-based drugs such as cisplatin playing a pivotal role in the management of solid tumors, and lobaplatin being crucial in the treatment of certain hematologic malignancies.[2] These platinum compounds primarily exert their therapeutic effects by binding to DNA, resulting in structural alterations that disrupt cellular integrity and induce apoptotic cell death.[3] However, despite their clinical success, platinum-based chemotherapeutics are associated with significant drawbacks, most notably their high toxicity to normal cells.[4] This nonselective cytotoxicity leads to a wide range of adverse side effects, which can severely affect patients' quality of life during treatment. As a result, there has been increasing interest in developing alternative therapeutic strategies for cancer treatment. One promising approach is the development of novel metal-based anticancer agents by replacing platinum with alternative metals, while also exploring a variety of ligand architectures.[5–8] For example, palladium, a member of the platinum-group metals, has emerged as a potential candidate for anticancer drug development, due to its structural and mechanistic similarities to platinum-based compounds.[9,10] Ruthenium and iridium have been investigated for their potential in photodynamic therapy, owing to their unique photophysical and redox properties.[11–15]

Rhodium is another member of the platinum-group metals that has traditionally been employed in catalytic processes.[16] In recent years, it has attracted growing attention due to its versatile coordination chemistry and potential biological activities.[17–20] The pharmacological properties of rhodium complexes are heavily influenced by their ligand design, with bidentate ligands, such as N^N,[21–24] N^C,[25–27] N^O[28] or N^S,[29] as well as *N*-heterocyclic carbene (NHC) ligands,[30–33] being particularly prevalent in medicinal rhodium chemistry. In our previous studies, we developed a series of cyclometalated octahedral Rh(III) complexes that demonstrated DNA-binding properties.[34] More recently, we have designed novel square-planar Rh(I) complexes incorporating tridentate ligands, which exhibit a particularly notable impact on breast adenocarcinoma.[35] Tridentate ligand tpy is a well-established scaffold in medicinal inorganic chemistry, known for its diverse biological activities and attractive features in metal-N^N^N complexes.[36] However, terpyridine-functionalized rhodium complexes remain largely unexplored in the context of anticancer drug development.[37] In the present study, we aim to design and synthesize a series of octahedral Rh(III) complexes, utilizing terpyridine as a N^N^N tridentate ligand in combination with various N^N-bidentate auxiliary ligands. This work will encompass the synthesis, characterization, and

[a] *H. Liang, H. Hong, L. Gao, S. Wang, Y. Shen, Prof. Y. Wang*
Chongqing Key Lab of Medicinal Chemistry & Molecular Pharmacology, School of Pharmacy and Bioengineering, Chongqing University of Technology, Chongqing 400054, P. R. China
E-mail: hrliang@cqut.edu.cn
shenbmy@cqut.edu.cn
wangyqnn@cqut.edu.cn

[b] *G. Wang*
School of Life Sciences, Nanjing University, Nanjing 210023, P. R. China

Supporting information for this article is available on the WWW under https://doi.org/10.1002/slct.202503583

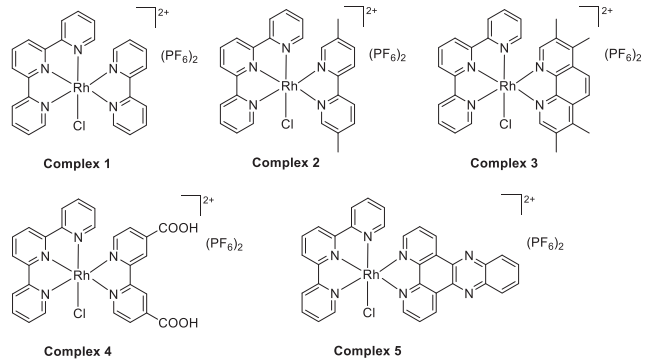

Scheme 1. Structures of the five complexes in this work.

evaluation of the anticancer efficacy of these complexes against a panel of human cancer cell lines.

2. Results and Discussion

2.1. Synthesis and Characterization

A series of five rhodium(III) complexes **1**–**5** with the general formula [Rh(tpy)(N^N)Cl](PF$_6$)$_2$ were synthesized by refluxing [Rh(tpy)Cl$_3$] with the respective N^N bidentate ligands in H$_2$O/EtOH, followed by addition of excess NH$_4$PF$_6$ to precipitate the products (Scheme 1). After purification by recrystallization from acetonitrile/diethyl ether, complexes were obtained as air-stable, crystalline solids in moderate yields ranging from 64% to 78%. All complexes demonstrated good solubility in polar organic solvents, including acetonitrile, acetone, and DMSO, but were insoluble in nonpolar solvents such as petroleum ether and diethyl ether. This solubility profile is consistent with their ionic character and suggests potential compatibility with biological testing conditions.

The molecular structures of complexes **1**–**5** were fully characterized using HR-MS, NMR, IR, and CHN elemental analysis. Complete spectroscopic data for all complexes are available in the Supporting Information (Figures S1–S5). All complexes showed intense peaks corresponding to the [M + H]$^+$ cation, with experimental *m/z* values matching theoretical calculations (Figures S6–S10). Key vibrational bands in the IR spectra of the complexes were observed at 1602–1606 cm^{-1} (C═N stretch) and 830–835 cm^{-1} (PF$_6^-$ counterion), confirming the proposed structures (Figure S11). The identity and purity of each complex were further confirmed by satisfactory elemental analysis.

To evaluate the stability of the complexes, a time-dependent ^{1}H NMR spectroscopic stability study was conducted in a mixture of 85% DMSO-d_6 / 15% phosphate-buffered saline (PBS) (pH ≈ 7.2, prepared from D$_2$O) at 37 °C. No significant changes were observed over a 48-h period, indicating that the structural integrity of the Rh center and its coordinated ligands is maintained under conditions that approximate the intracellular environment (Figure S12).

Single crystal of complex **5** [Rh(tpy)(dppz)Cl](PF$_6$)$_2$ suitable for X-ray diffraction analysis was obtained through slow vapor diffusion of diethyl ether into the acetonitrile solution at ambient temperature. The crystal structure (Figure 1, Table S1) unequivocally confirms the octahedral coordination geometry around the Rh(III) center, with the tpy adopting its characteristic meridional tridentate binding mode (N^N^N), while the dppz ligand chelates through its N^N donor atoms. The chloride ligand completes the coordination sphere, occupying the sixth position. Structural analysis reveals a near-ideal octahedral geometry, evidenced by cis-angles ranging from 80.50(15)° to 99.84(15)° and trans-angles between 161.57(16)° and 179.22(16)°, with the Rh-N bond lengths showing remarkable consistency [1.959(4)-2.041(4) Å (Rh-tpy), 2.046(4)-2.047(4) Å (Rh-dppz)] that are significantly shorter than the Rh—Cl bond length of 2.3211(12) Å, reflecting the different trans influences of the coordinated ligands. The tpy ligand imposes considerable geometric constraint, manifested by nearly identical N—Rh—N bite angles of 80.98(17)° and 80.62(16)°, while the overall structure displays pronounced rigidity due to the planar aromatic systems of both tpy and dppz ligands. The relatively short Rh—N bonds, particularly to the central pyridine of the tpy ligand (1.959(4) Å), suggest strong metal-ligand interactions that may contribute to the complex's stability. The crystallographic data have been deposited with the Cambridge Crystallographic Data Centre (CCDC no. 2442291).

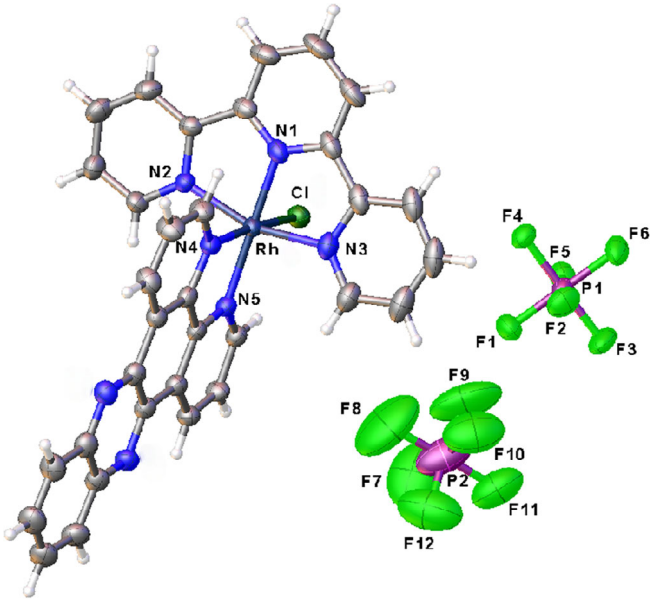

Figure 1. X-ray crystal structure for complex **5**.

2.2. Antitumor Efficacy of Complexes 1–5

To evaluate the antitumor therapeutic potential of complexes **1**–**5**, their anti-proliferative activity was assessed using an in vitro MTT assay across four tumor cell lines: AGS (human gastric adenocarcinoma), MCF-7 (human breast adenocarcinoma), HeLa (human cervical adenocarcinoma), and HepG2 (human hepatocellular carcinoma). Additionally, a non-tumor cell line, GES-1 (human gastric epithelial cells), was included for comparative purposes. Cisplatin served as the positive control for

Table 1. IC_{50} and selectivity index (SI) of complexes **1**–**5** against different cell lines.[a)]

Cell Lines	AGS		MCF-7		HeLa		HepG-2		GES-1	
–	IC_{50} (μM)	SI	IC_{50} (μM)	SI	IC_{50} (μM)	SI	IC_{50} (μM)	SI	IC_{50} (μM)	SI
Complex **1**	46.6 ± 1.7	2.1	>100	–	>100	–	>100	–	>100	–
Complex **2**	37.7 ± 2.1	2.7	>100	–	>100	–	>100	–	>100	–
Complex **3**	7.0 ± 0.6	1.0	9.3 ± 1.1	0.7	5.4 ± 1.1	1.3	21.4 ± 4.3	0.3	6.9 ± 0.3	–
Complex **4**	>100	–	>100	–	>100	–	>100	–	>100	–
Complex **5**	8.3 ± 0.8	2.5	13.9 ± 1.5	1.5	23.6 ± 2.3	0.9	34.1 ± 4.0	0.6	20.5 ± 1.3	–
Cisplatin	38.8 ± 3.8	1.1	14.8 ± 2.5	2.8	24.8 ± 3.8	1.7	13.5 ± 1.5	3.1	42.1 ± 3.1	–

[a)] Data are shown as mean ± SD (n = 3); SI (Selectivity index) = IC_{50} (non-tumor cells)/IC_{50} (tumor cells).

this experiment. Following a 48-hour incubation of the cell lines with varying concentrations of complexes **1**–**5**, cell viability was measured using the MTT assay, and the results are summarized in Table 1. Notably, complexes **3** and **5** exhibited higher anti-proliferative activity than complexes **1**, **2**, and **4**.

The selectivity index (SI), reflecting the therapeutic window of the complex, was calculated to evaluate their preferential suppression of malignant cell viability over normal cells. Despite showing potent inhibitory effects on cell viability in both tumor and non-tumor cells, complex **3** exhibited a narrow therapeutic window due to insufficient selectivity, which may limit its future clinical applications. In contrast, complex **5** demonstrated a promising therapeutic profile, with a notably low IC_{50} and a favorable SI. When compared to cisplatin, complex **5** exhibited higher selectivity towards AGS cells and a significantly lower IC_{50}, suggesting that it may offer superior therapeutic potential in the treatment of gastric adenocarcinoma.

2.3. Molecular Docking Studies

DNA is a well-established molecular target for many metal-based anticancer agents. To investigate the DNA-binding interactions of the synthesized Rh(III) complexes, molecular docking studies were conducted using the Surflex-Dock algorithm with ctDNA as the target (PDB ID: 1LU5). Validation of the docking protocol was confirmed by redocking the co-crystallized ligand (cyclohexylamine), yielding a root-mean-square deviation (RMSD) of 0.676 Å, thereby confirming the reliability of the docking approach (Figure S13).

All five complexes adopted similar binding poses, primarily engaging the DNA minor groove through dipole–dipole interactions between the electron-deficient Rh(III) center and the electron-rich nitrogen atoms on guanine bases, particularly dG-16. Complexes **3** and **5** exhibited slightly shorter Rh···N distances (~4.7 Å) compared to complexes **1**, **2**, and **4** (~4.9–5.0 Å), correlating with their lower IC_{5n} values and enhanced cytotoxic activity. In contrast, cisplatin displayed stronger interactions (distances of ~2.6–2.7 Å) due to its smaller molecular volume (~89.1 $Å^3$), enabling deeper insertion into the DNA groove. However, its greater flexibility may reduce binding specificity. By comparison, complexes **3** (390.6 $Å^3$) and **5** (413.2 $Å^3$) demonstrated an optimal molecular size and rigidity, facilitating effective intercalation into the minor groove and likely impeding DNA replication. These docking results support the hypothesis that minor groove binding contributes significantly to the observed cytotoxicity, especially for complexes **3** and **5**, and are in line with the experimental antiproliferative data (Figure 2).

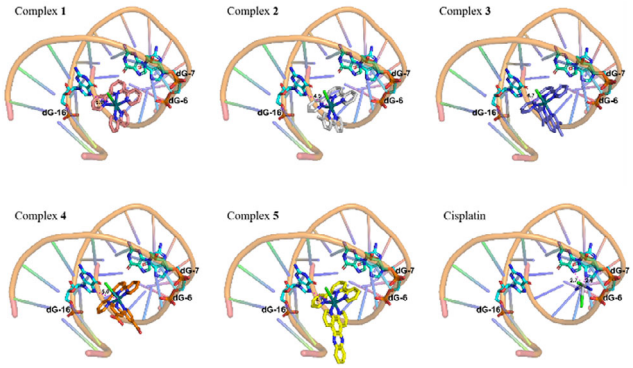

Figure 2. The binding mode between complexes and ctDNA.

2.4. Complex 5 Induced Apoptosis in AGS

To elucidate the mechanism underlying the anti-proliferative effects of complex **5** on AGS cells, its ability to trigger apoptosis was assessed via Annexin V-FITC/PI dual staining followed by flow cytometry. AGS cells were exposed to increasing concentrations of complex **5** (5, 10, and 15 μM) for 24 h As shown in Figure 3, a dose-dependent escalation in apoptotic cell populations was observed. At 5 μM, the early and late-stage apoptosis rates were 17.34% and 15.10%, respectively. When the concentration of complex **5** was increased to 10 μM, these apoptosis rates rose to 21.29% and 19.58%, respectively, and at 15 μM, the rates increased further to 26.35% and 34.62%. These data indicate that apoptosis induction contributes to the reduction of AGS cells' viability by complex **5**.

2.5. Complex 5 Induced S Phase Cell Cycle Arrest in AGS

The effect of complex **5** on the cell cycle was also examined (Figure 4). Flow cytometry analysis revealed that complex **5**

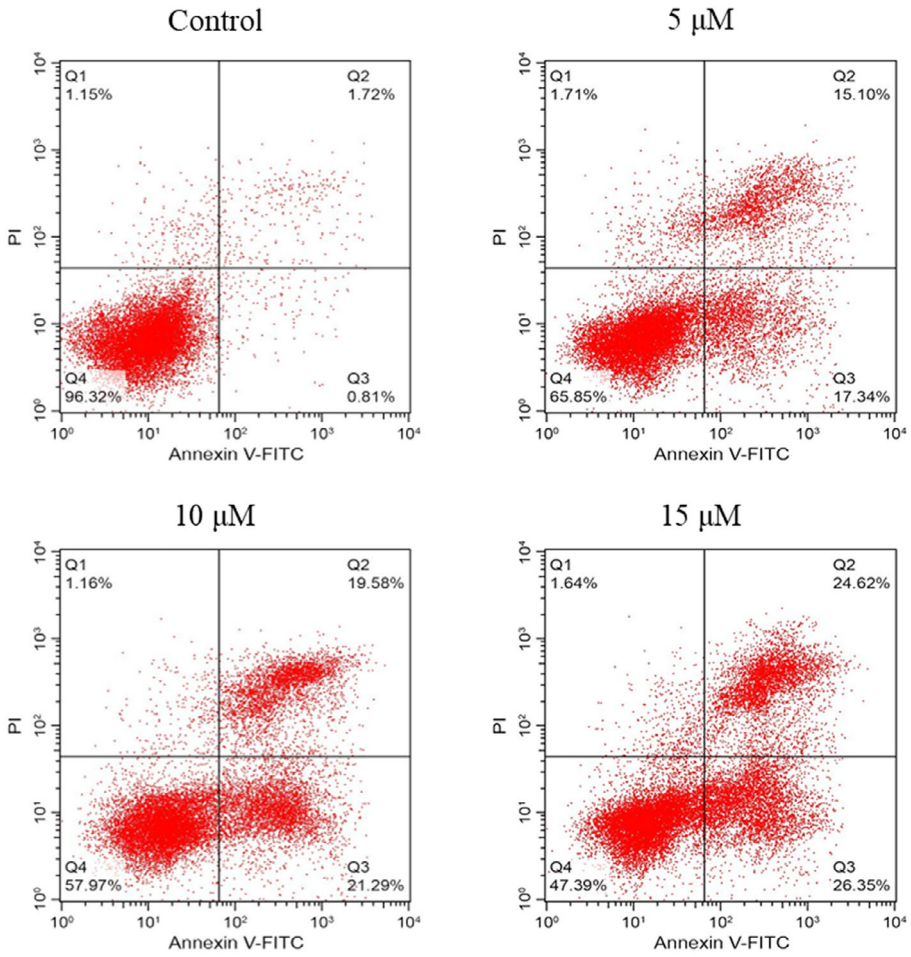

Figure 3. Complex **5** induced apoptosis in AGS cells. Apoptotic rates were measured by Annexin V/PI staining after 24 h treatment with 5–15 μM complex **5**. Data are shown as mean ± SD (n = 3).

induced a concentration-dependent arrest of the AGS cell cycle at the S phase. As the concentration of complex **5** increased, the proportion of cells in the G0/G1 phase decreased from 58.5% to 30.1%, while the proportion in the S phase increased from 31.1% to 68.4%. Additionally, the G2/M phase population decreased from 10.4% to 1.5%. At the highest concentration of complex **5** tested, the S-phase population increased by 37.3% compared to the control group. These findings strongly suggest that complex **5** effectively arrests the AGS cell cycle at the S phase, thereby inhibiting cell proliferation.

2.6. Complex 5 Increased ROS Levels in AGS

To investigate the potential mechanism behind the anticancer activity of complex **5**, its effect on intracellular reactive oxygen species (ROS) levels was evaluated. AGS cells were treated with varying concentrations of complex **5** for 24 h, and ROS levels were measured using a fluorescence-based assay. As shown in Figure 5, complex **5** induced a concentration-dependent increase in ROS levels compared to the untreated control group. These findings indicate that complex **5** elevates intracellular ROS levels in AGS cells, which may contribute to its anticancer activity by inducing oxidative stress.

3. Conclusion

We have synthesized and structurally characterized five new octahedral rhodium(III) complexes bearing terpyridine and diverse bidentate N-donor ligands. Among them, complex **5** displayed superior cytotoxicity and selectivity toward gastric adenocarcinoma cells. Mechanistic studies confirmed its ability to bind DNA, arrest the cell cycle in S-phase, elevate ROS levels, and trigger apoptosis. The combination of structural rigidity, favorable DNA-binding properties, and selective anticancer activity positions these terpyridine-functionalized Rh(III) complexes—particularly complex **5**—as attractive candidates for further investigation as metal-based chemotherapeutics.

4. Experimental Section

4.1. Materials and Methods

The synthesis of dppz followed the reported procedure.[32] All other materials were obtained from commercial sources and were used without further purification. NMR spectra were recorded on a Bruker AVANCE III HD-400 MHz. NMR instrument operating at room temperature (400 MHz for ^{1}H and 101 MHz for ^{13}C). Referencing is relative to tetramethylsilane. High-resolution mass spectra were recorded on a

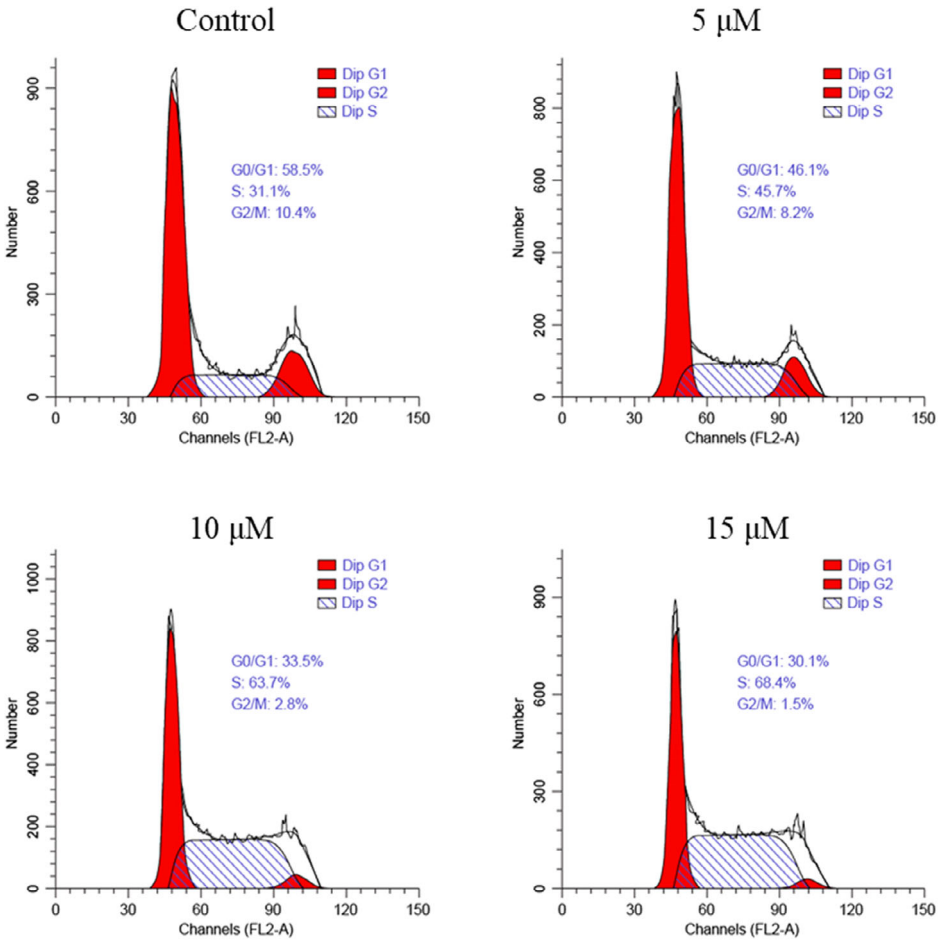

Figure 4. The distribution of the AGS cell cycle induced by complex **5** at the concentrations of 5 μM, 10 μM, and 15 μM.

Shimadzu LCMS-IT-TOF high-resolution liquid chromatograph. Samples for microanalysis were dried in vacuo to constant weight (20 °C, ca. 0.1 torr) and analyzed on a Flash EA 111 CHN elemental analyzer. FT-IR spectra (4000–400 cm^{-1}) were recorded at room temperature using a NEXUS 670 spectrophotometer.

Complex 1. $RhCl_3{\cdot}3H_2O$ (0.395 g, 1.5 mmol) and tpy (0.350 g, 1.5 mmol) in EtOH (10 mL) were refluxed for 2 h. Cooled to room temperature, the product was filtered off and washed with H_2O, EtOH and diethyl ether successively, and then dried in vacuo to give the $Rh(tpy)Cl_3$. The product was used in subsequent reactions without further purification. $Rh(tpy)Cl_3$ (0.088 g, 0.2 mmol) and 2,2′-bipyridine (bpy) (0.039 g, 0.25 mmol) in a mixture of H_2O/EtOH (1:1, 10 mL) were refluxed for 4 h. NH_4PF_6 (1.6 g, 9.8 mmol) and H_2O (20 mL) were then added into the solution, and the reaction mixture was refluxed for 2 h. Cooled to room temperature, the product was filtered off. The crude product was dissolved in acetonitrile (5 mL) and recrystallized by the slow addition of diethyl ether (10 mL) to yield the desired compound as a yellow solid, which was dried in vacuo. Yield = 0.120 g, 74%. HR-MS (ESI+): calcd for $[M + H]^+$, 817.9746; found, 817.9872. Elem. Anal. Calcd for $C_{25}H_{19}ClF_{12}N_5P_2Rh$: C, 36.72; H, 2.34; N, 8.56. Found C, 36.63; H, 2.23; N, 8.68. ^1H NMR (400 MHz, DMSO-d_6) δ 9.76 (d, $J = 1.7$ Hz, 1H), 9.12 (d, $J = 8.1$ Hz, 3H), 8.96–8.89 (m, 4H), 8.78 (td, $J = 7.9$, 1.5 Hz, 1H), 8.42 (td, $J = 7.9$, 1.4 Hz, 2H), 8.33 – 8.27 (m, 2H), 7.85 (d, $J = 5.6$ Hz, 3H), 7.67 (ddd, $J = 7.4$, 5.6, 1.4 Hz, 2H), 7.50 (ddd, $J = 7.4$, 5.8, 1.4 Hz, 1H). $^{13}C\{^1H\}$ NMR (101 MHz, DMSO-d_6) δ 156.97, 155.92, 154.58, 152.99, 151.75, 151.26, 143.69, 142.94, 142.61, 142.39, 130.29, 129.73, 127.24, 126.96, 126.73, 126.19. IR (solid): ν = 1605 cm^{-1} (ν(C═N)), ν = 833 cm^{-1} ($\nu(PF_6^-)$).

Complex 2. This was prepared following the above procedure for complex **1**, except that 5,5′-dimethyl-2,2′-dipyridy (dmbpy) (0.047 g, 0.25 mmol) was used in place of 2,2′-bipyridine. Yield = 0.120 g (yellow solid), 71%. HR-MS (ESI+): calcd for $[M + H]^+$, 846.0059; found, 846.5205. Elem. Anal. Calcd for $C_{27}H_{23}ClF_{12}N_5P_2Rh$: C, 38.34; H, 2.74; N, 8.28. Found C, 38.26; H, 2.68; N, 8.37. ^1H NMR (400 MHz, DMSO-d_6) δ 9.51 (d, $J = 1.9$ Hz, 1H), 9.11 (d, $J = 8.1$ Hz, 2H), 8.94 (ddd, $J = 8.0$, 4.7, 3.4 Hz, 4H), 8.75 (d, $J = 8.4$ Hz, 1H), 8.59 (dd, $J = 8.4$, 1.9 Hz, 1H), 8.42 (td, $J = 7.9$, 1.5 Hz, 2H), 8.12 (d, $J = 8.3$ Hz, 1H), 7.85 (d, $J = 5.5$ Hz, 2H), 7.67 (ddd, $J = 7.4$, 5.6, 1.4 Hz, 2H), 7.56 (s, 1H), 2.70 (s, 3H), 2.14 (s, 3H). $^{13}C\{^1H\}$ NMR (101 MHz, DMSO-d_6) δ 157.15, 154.71, 153.45, 152.89, 151.26, 150.52, 143.46, 143.09, 142.83, 142.50, 140.56, 130.20, 127.24, 126.96, 125.67, 19.24, 18.62. IR (solid): ν = 1606 cm^{-1} (ν(C═N)), ν = 830 cm^{-1} ($\nu(PF_6^-)$).

Complex 3. This was prepared following the above procedure for complex **1**, except that 3,4,7,8-tetramethyl-1,10-phenanthroline (TMPhen) (0.060 g, 0.25 mmol) was used in place of 2,2′-bipyridine. Yield = 0.141 g (pale yellow solid), 78%. HR-MS (ESI+): calcd for $[M + H]^+$, 898.0372; found, 898.3321. Elem. Anal. Calcd for $C_{31}H_{27}ClF_{12}N_5P_2Rh$: C, 41.47; H, 3.03; N, 7.80. Found C, 41.38; H, 2.95; N, 7.88. ^1H NMR (400 MHz, DMSO-d_6) δ 9.70 (s, 1H), 9.14 (d, $J = 8.2$ Hz, 2H), 8.95 (t, $J = 7.9$ Hz, 3H), 8.70 (d, $J = 9.4$ Hz, 1H), 8.51 (d, $J = 9.5$ Hz, 1H), 8.36 (td, $J = 7.9$, 1.4 Hz, 2H), 7.91 (s, 1H), 7.68 (d, $J = 5.6$ Hz, 2H), 7.50 (ddd, $J = 7.3$, 5.6, 1.3 Hz, 2H), 3.08 (s, 3H), 2.83 (s, 3H), 2.75 (s, 3H), 2.27 (s, 3H). $^{13}C\{^1H\}$ NMR (101 MHz, DMSO-d_6) δ 157.05, 154.93, 153.50, 149.50, 143.83, 142.60, 140.19, 138.07, 137.50, 133.62, 132.05, 131.40, 130.04, 127.21, 25.96, 22.57. IR (solid): ν = 1602 cm^{-1} (ν(C═N)), ν = 832 cm^{-1} ($\nu(PF_6^-)$).

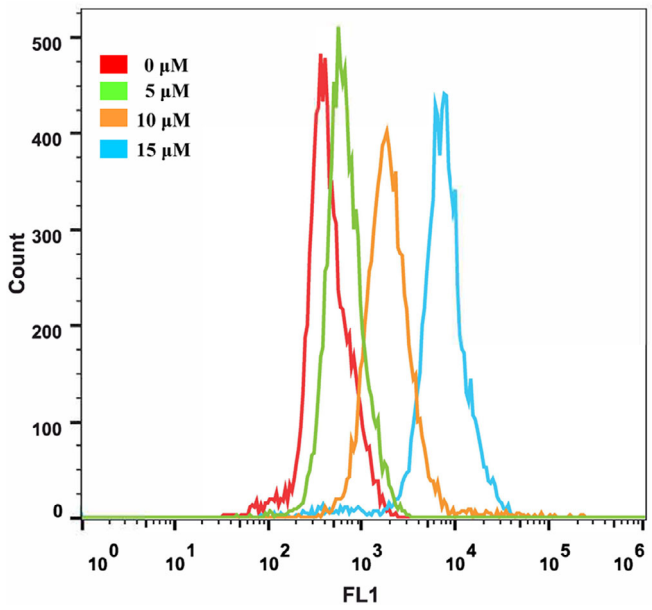

Figure 5. The levels of ROS with AGS cells induced by complex **5** at the concentrations of 5 μM, 10 μM, and 15 μM.

Complex 4. This was prepared following the above procedure for complex **1**, except that 2,2′-bipyridine-4,4′-dicarboxylic acid (dcbpy) (0.061 g, 0.25 mmol) was used in place of 2,2′-bipyridine. Yield = 0.120 g (pale yellow solid), 66%. HR-MS (ESI+): calcd for $[M + H]^+$, 905.9542; found, 906.2628. Elem. Anal. Calcd for $C_{27}H_{19}ClF_{12}N_5O_4P_2Rh$: C, 35.80; H, 2.11; N, 7.73. Found C, 35.73; H, 2.03; N, 7.82. ^{1}H NMR (400 MHz, DMSO-d_6) δ 9.89 (d, J = 5.8 Hz, 1H), 9.56 (s, 1H), 9.33 (s, 1H), 9.13 (d, J = 8.0 Hz, 2H), 8.95 (dd, J = 8.1, 3.4 Hz, 3H), 8.65 (dd, J = 5.8, 1.7 Hz, 1H), 8.41 (t, J = 7.9, 1.4 Hz, 2H), 7.94 (dd, J = 15.0, 5.7 Hz, 3H), 7.74 (dd, J = 6.0, 1.7 Hz, 1H), 7.68–7.63 (m, 2H). ^{13}C{^{1}H} NMR (101 MHz, DMSO-d_6) δ 165.31, 164.61, 156.89, 156.46, 154.62, 153.29, 152.07, 143.83, 142.61, 130.24, 129.53, 127.26, 126.97, 126.34, 25.96. IR (solid): ν = 1602 cm^{-1} (ν(C═N)), ν = 832 cm^{-1} (ν(PF_6^-)).

Complex 5. This was prepared following the above procedure for complex **1**, except that dppz (0.070 g, 0.25 mmol) was used in place of 2,2′-bipyridine. Yield = 0.120 g (pale yellow solid), 64%. HR-MS (ESI+): calcd for $[M + H]^+$, 943.9964; found, 944.1374. Elem. Anal. Calcd for $C_{33}H_{21}ClF_{12}N_7P_2Rh$: C, 41.99; H, 2.24; N, 10.39. Found C, 41.92; H, 2.17; N, 10.46. ^{1}H NMR (400 MHz, DMSO-d_6) δ 10.20 (d, J = 7.9 Hz, 1H), 10.13 (d, J = 5.4 Hz, 1H), 9.74 (d, J = 7.9 Hz, 1H), 9.18 (d, J = 8.2 Hz, 2H), 8.99 (dd, J = 10.5, 8.1 Hz, 3H), 8.79 (dd, J = 8.3, 5.4 Hz, 1H), 8.64 (dd, J = 7.7, 2.1 Hz, 1H), 8.55 (dd, J = 8.2, 1.8 Hz, 1H), 8.42 – 8.35 (m, 3H), 8.27 (ddd, J = 8.0, 5.8, 1.8 Hz, 2H), 7.99 (dd, J = 8.2, 5.5 Hz, 1H), 7.85 (d, J = 5.6 Hz, 2H), 7.59 (ddd, J = 7.4, 5.6, 1.3 Hz, 2H). ^{13}C{^{1}H} NMR (101 MHz, DMSO-d_6) δ 157.05, 154.93, 153.49, 149.84, 149.50, 142.60, 140.19, 139.86, 138.08, 137.50, 133.69, 132.05, 131.40, 130.04, 129.20, 127.21, 127.04. IR (solid): ν = 1606 cm^{-1} (ν(C═N)), ν = 835 cm^{-1} (ν(PF_6^-)).

4.2. X-ray Crystallography

Diffraction data of complex $[Rh(tpy)(dppz)Cl](PF_6)_2$ was measured at 196.0 K using MoKα radiation (λ = 0.71,073 Å) on a Bruker APEX-II CCD diffractometer. Using Olex2, the structure was solved with the ShelXT structure solution program using Intrinsci Phasing and refined with the ShelXL refinement package using Least Squares minimisation.[38,39]

4.3. Cell Culture

Tumor cell lines AGS, MCF-7, HeLa, HepG2, and non-tumor cell line GES-1 were purchased from the China Center for Type Culture Collection. AGS and GES cells were cultured in Roswell Park Memorial Institute 1640 medium (RPMI 1640), while MCF-7, HeLa, and HepG2 cells were maintained in Dulbecco's modified Eagle's medium (DMEM). All media were supplemented with 10% fetal bovine serum (FBS), 100 U/mL penicillin, and 100 μg/mL streptomycin, and cells were incubated in a humidified atmosphere with 5% CO_2 at 37 °C.

4.4. Anti-proliferation Assay

The anti-proliferation effect of complexes **1**–**5** was evaluated by the 3-(4,5-dimethylthiazol-2-yl)-2,5-diphenyltetrazolium bromide (MTT) colorimetric assay as described previously. AGS, MCF-7, HeLa, HepG-2, and GES-1 cells (7000 cells/well) were seeded into 96-well plates and incubated overnight. The cells were incubated with complexes (1–100 μM) or cisplatin, with 0.5% DMSO as vehicle control. MTT solution (0.5 mg/mL final) was added for 4 h at 37 °C. The medium was aspirated, and formazan crystals were dissolved in DMSO. Absorbance at 490 nm was measured, and viability was normalized to controls.

4.5. Molecular Docking Method

The method used to explore the binding mode between design compounds and ctDNA could be referenced from our previous study.[35] The binding site of ctDNA (ww.rcsb.org, ID: 1LU5) was defined using SYBYL-X based on the co-crystal ligand, and the volume of the pocket and compounds were determined by MOLCAD with the Fast Connolly method.[26] The structure of all complexes was optimized with the Tripos force field and MMFF95 charge. The docking program Surflex-Dock GeomX (SFXC) in SYBYL-X was used to dock the complexes into the pocket. The main protocols or parameters of docking were addressed in our previous publications.[40] Briefly, the docking parameters were as follows: (a) the "number of starting conformations per ligand" was set to 10, and the "number of max conformations per fragment" was set to 20; (b) the "maximum number of rotatable bonds per molecule" was set to 100; (c) flags were turned on at "pre-dock minimization", "post-dock minimization", "molecule fragmentation", and "soft grid treatment"; (d) "activate spin alignment method with density of search" was set to 9.0; and (e) the "number of spins per alignment" was set to 12. To validate the docking program, we redocked the co-crystal ligand and calculated the RMSD based on their superimposition.

4.6. Apoptosis Analysis by Annexin V/PI Staining

AGS cells (2×10^5/well) were seeded in 6-well plates and cultured overnight. Cells were treated with complex **5** (5, 10, and 15 μM) for 24 h, harvested, washed, and resuspended in pre-cooling PBS. Apoptosis was quantified using an Annexin V-FITC/PI Apoptosis Detection Kit (Beyotime, C1062m) per the manufacturer's protocol. Briefly, cells were stained with FITC-conjugated Annexin V and PI for 15 min in the dark, followed by immediate analysis on a FACSCalibur flow cytometer (BD FACSAria SORP). Data were processed with FlowJo software (FlowJo 10.8.1).

4.7. Cell Cycle Analysis

AGS cells (2×10^5/well) were seeded in 6-well plates and allowed to adhere overnight. Cells were treated with complex **5** (5, 10, or 15 μM) for 24 h, harvested, and fixed in 70% ice-cold ethanol. After fixation, cells were incubated with 100 μg/mL RNase A at 37 °C for 30 min, followed by staining with 50 μg/mL propidium iodide (PI) for 30 min on ice in the dark. Cell cycle distribution was analyzed using a FACSCalibur flow cytometer (BD FACSAria SORP), and data were processed with FlowJo software (FlowJo 10.8.1).

4.8. ROS Determination

Following treatment with complex **5** (5–15 μM, 24 h), cells were harvested and incubated with 10 μM DCFH-DA in PBS for 20 min at room temperature in the dark. After washing three times with PBS, cell suspensions were filtered through a 70-μm nylon mesh to remove aggregates. Intracellular ROS levels were analyzed using a flow cytometer with excitation/emission settings of 488/530 nm (FL1 channel). Data were processed with FlowJo software (FlowJo 10.8.1).

Supporting Information

^{1}H and ^{13}C{1H} NMR spectra, HRMS spectra, FT-IR spectra, crystallographic data, and cell apoptosis data.

Acknowldgements

This work was supported by the Science and Technology Research Program of Chongqing Municipal Education Commission (Grant No. KJQN202201167).

Conflict of Interests

The authors declare no conflict of interest.

Data Availability Statement

The data that support the findings of this study are available in the supplementary material of this article.

Keywords: Anticancer agent · Octahedral complex · Rhodium · Terpyridine

[1] F. Bray, M. Laversanne, H. Sung, J. Ferlay, R. L. Siegel, I. Soerjomataram, A. Jemal, *CA Cancer J. Clin.* **2024**, *74*, 229–263.
[2] P. M. Bruno, Y. Liu, G. Y. Park, J. Murai, C. E. Koch, T. J. Eisen, J. R. Pritchard, Y. Pommier, S. J. Lippard, M. T. Hemann, *Nat. Med.* **2017**, *23*, 461–471.
[3] B. J. Pages, D. L. Ang, E. P. Wright, J. R. Aldrich-Wright, *Dalton Trans.* **2015**, *44*, 3505–3526.
[4] I. Romero-Canelón, P. J. Sadler, *Inorg. Chem.* **2013**, *52*, 12276–12291.
[5] T. S. Prathima, B. Choudhury, M. G. Ahmad, K. Chanda, M. M. Balamurali, *Coord. Chem. Rev.* **2023**, *490*, 215231.
[6] S. De, S. Kazi, S. Banerjee, S. Banerjee, N. Sarkar, S. Kumar Shah, Y.-C. Kuo, S. K. Ashok Kumar, *Coord. Chem. Rev.* **2024**, *498*, 215462.
[7] Z.-F. Wang, X.-F. Zhou, Q.-C. Wei, Q.-P. Qin, J.-X. Li, M.-X. Tan, S.-H. Zhang, *Eur. J. Med. Chem.* **2022**, *238*, 114418.
[8] Y. Chen, X. Hu, L. Yuan, S. Zhang, H. Ma, *J. Mol. Struct.* **2025**, *1340*, 142499.
[9] M. Vojtek, M. P. M. Marques, I. M. P. L. V. O. Ferreira, H. Mota-Filipe, C. Diniz, *Drug Discov. Today* **2019**, *24*, 1044–1058.
[10] R. Czarnomysy, D. Radomska, O. K. Szewczyk, P. Roszczenko, K. Bielawski, *Int. J. Mol. Sci.* **2021**, *22*, 8271.
[11] R. Guan, L. Xie, L. Ji, H. Chao, *Eur. J. Inorg. Chem.* **2020**, 3978–3986.
[12] J. Shen, T. W. Rees, L. Ji, H. Chao, *Coord. Chem. Rev.* **2021**, *443*, 214016.
[13] Y. Wu, S. Li, Y. Chen, W. He, Z. Guo, *Chem. Sci.* **2022**, *13*, 5085–5106.
[14] R. Das, U. Das, N. Roy, C. Mukherjee, S. U, P. Paira, *Dyes Pigm.* **2024**, *226*, 112134.
[15] N. Manav, A. Janaagal, I. Gupta, *Coord. Chem. Rev.* **2024**, *511*, 215798.
[16] H. Fang, Z. Sun, M. Xu, W. Xue, Z. Qian, Z. Li, C. Zhang, Q. Wu, J. Xu, R. Li, H. Fu, X. Zheng, H. Chen, *Ind. Eng. Chem. Res.* **2025**, *64*, 1488–1496.
[17] I. Audzeyenka, A. Piwkowska, D. Rogacka, M. Makowski, M. Kowalik, *J. Med. Chem.* **2024**, *67*, 21364–21379.
[18] C. G. L. Nongpiur, C. Soh, D. F. Diengdoh, A. K. Verma, R. Gogoi, V. Banothu, W. Kaminsky, M. R. Kollipara, *J. Organomet. Chem.* **2023**, *998*, 122788.
[19] E. Skelton, U. Erasquin, A. Sukul, A. Zuercher, J. White, B. J. Bythell, K. L. A. Cimatu, *Inorg. Chem.* **2023**, *62*, 3368–3380.
[20] N. Toupin, M. K. Herroon, R. P. Thummel, C. Turro, I. Podgorski, H. Gibson, J. J. Kodanko, *Chem. -Eur. J.* **2022**, *28*, e202104430.
[21] W. Li, S. Li, M. Zhu, G. Xu, X. Man, Z. Zhang, H. Liang, F. Yang, *J. Med. Chem.* **2024**, *67*, 17243–17258.
[22] M. Kowalik, J. Masternak, M. Olszewski, N. Maciejewska, K. Kazimierczuk, J. Sitkowski, A. M. Dąbrowska, A. Chylewska, M. Makowski, *Inorg. Chem.* **2024**, *63*, 1296–1316.
[23] W. K. Chu, C. K. Rono, B. C. E. Makhubela, *Eur. J. Inorg. Chem.* **2024**, *27*, e202300541.
[24] L. Guo, P. Li, J. Li, Y. Gong, X. Li, Y. Liu, K. Yu, Z. Liu, *Inorg. Chem.* **2023**, *62*, 15118–15137.
[25] Y. Zheng, X.-X. Chen, D.-Y. Zhang, W.-J. Wang, K. Peng, Z.-Y. Li, Z.-W. Mao, C.-P. Tan, *Chem. Sci.* **2023**, *14*, 6890–6903.
[26] A. Nahaei, Z. Mandegani, S. Chamyani, M. Fereidoonnezhad, H. R. Shahsavari, N. Y. Kuznetsov, S. M. Nabavizadeh, *Inorg. Chem.* **2022**, *61*, 2039–2056.
[27] W.-Y. Zhang, H. E. Bridgewater, S. Banerjee, J. J. Soldevila-Barreda, G. J. Clarkson, H. Shi, C. Imberti, P. J. Sadler, *Eur. J. Inorg. Chem.* **2020**, 1052–1060.
[28] Z.-F. Wang, X.-L. Nai, Y. Xu, F.-H. Pan, F.-S. Tang, Q.-P. Qin, L. Yang, S.-H. Zhang, *Dalton Trans.* **2022**, *51*, 12866–12875.
[29] L. Rafols, M. Azmanova, N. Perrigault, P. A. Cooper, S. D. Shnyder, W. H. C. Martin, A. Pitto-Barry, *J. Organomet. Chem.* **2024**, *1013*, 123168.
[30] J. Schmidt, J. Wölker, P. Lippmann, I. Ott, *J. Organomet. Chem.* **2022**, *964*, 122300.
[31] V. Tolga Özdemir, S. Batıkan Kavukcu, A. Dila Çağlar, A. Nalbantsoy, H. Türkmen, *Inorg. Chem. Commun.* **2024**, *160*, 111963.
[32] M. O. Zouaghi, N. Amri, S. Hassen, Y. Arfaoui, N. Özdemir, I. Özdemir, N. Hamdi, *Inorg. Chim. Acta* **2023**, *551*, 121459.
[33] M. Olgun Karataş, T. Keskin, N. Özdemir, H. Küçükbay, S. Tekin, A. Mansur, S. Günal, S. Sandal, *Inorg. Chem. Commun.* **2022**, *146*, 110080.
[34] H. Liang, T. Hao, C. Yin, X. Yang, H. Fu, X. Zheng, R. Li, D. Xiao, H. Chen, *Eur. J. Inorg. Chem.* **2017**, *2017*, 4149–4157.
[35] H. Liang, W. Huang, X. Xu, D. Zou, Y. Wang, F. Yin, *Organometallics* **2024**, *43*, 108–118.
[36] R. R. Panicker, A. Sivaramakrishna, *Coord. Chem. Rev.* **2022**, *459*, 214426.
[37] A. Caković, D. Ćoćić, M. Živanović, N. Janković, N. Milivojević, M. Delibašić, M. Kostić, I. Radojević, M. Grujović, K. G. Marković, O. R. Klisurić, M. Vraneš, J. Bogojeski, *J. Med. Chem.* **2024**, *67*, 13349–13362.
[38] G. M. Sheldrick, *Acta Cryst.* **2015**, *A71*, 3–8.
[39] G. M. Sheldrick, *Acta Cryst.* **2015**, *C71*, 3–8.
[40] Y. Wang, W. Lin, N. Wu, S. Wang, M. Chen, Z. Lin, X.-Q. Xie, Z. Feng, *Acta Pharmacol. Sin.* **2019**, *40*, 1138–1156.

Manuscript received: June 24, 2025